Journal of Metamorphic Geology

WILEY

Journal of METAMORPHIC GEOLOGY

ORIGINAL ARTICLE OPEN ACCESS

A Cautionary Tale About Not 'Joining the Dots' to Infer Anticlockwise *P-T* Paths

Owen Weller[1] | Joseph Benson[1,2] | Alex Copley[1]

[1]Department of Earth Sciences, University of Cambridge, Cambridge, UK | [2]School of Earth and Environmental Sciences, University of St Andrews, St Andrews, UK

Correspondence: Owen Weller (ow212@cam.ac.uk)

Received: 3 September 2024 | **Revised:** 25 November 2024 | **Accepted:** 12 December 2024

Funding: This work was partly supported by Future Leaders Fellowship MR/V02292X/1 (O.W.) and NERC grant NE/W00562X/1 (A.C.).

ABSTRACT

Uncertainty surrounds the cause and interpretation of anticlockwise pressure-temperature (*P–T*) paths in metamorphic terranes. Here, we focus on the viability of a commonly proposed mechanism—magmatic heat transfer during thickening—using a case study of the Roineabhal terrane in Scotland, where such an anticlockwise *P–T* path has been proposed. Phase equilibria modelling of new samples, combined with previous *P–T* estimates, provides evidence for regional kyanite-grade granulite-facies metamorphism, with an additional spatially localised region of ultrahigh temperature conditions adjacent to an anorthosite intrusion. The spatial geometry of the ultrahigh temperature samples, combined with scaling arguments and thermal modelling of these results, shows that the ultrahigh temperature metamorphism is contact in nature and should not be joined to the regional metamorphism to infer an anticlockwise *P–T* path. Rather, the regional metamorphism features hairpin *P–T* loops, overlain adjacent to the anorthosite by a short-lived, high-temperature excursion. Because metamorphic rocks typically yield a fragmentary record during fluctuating thermal conditions, due to requiring hydration to maintain equilibrium during down-temperature evolution, it is critical to assess in this manner the thermal viability of the range of *P–T* paths that could connect the preserved assemblages. In general, intrusion radii of tens of kilometres, or repeated intrusions of smaller bodies in quick succession (e.g., <10 kyr for a 1-km radius), would be required for true magmatically driven anticlockwise *P–T* paths. Given the unlikely nature of these requirements in most tectonic settings, such anticlockwise *P–T* paths are likely to be rarer than reported. For many scenarios, *P–T* paths commonly interpreted as anticlockwise *P–T* paths are instead likely to take the form described in this study.

1 | Introduction

The thermal conditions experienced during metamorphism represent the interplay between crustal thickening and thinning, radiogenic heating, erosion and the intrusion of igneous bodies (England and Thompson 1984). Anticlockwise pressure–temperature (*P–T*) paths are rarer in the geological record than their clockwise counterparts, and their tectonic implications are debated. In extensional settings, isobaric cooling following peak-*T* conditions can occur at deep crustal levels due to the cooling following extension of the crust and mantle (e.g., Sandiford and Powell 1986). Depending on the prior history of a region, and whether prograde information is preserved, such isobaric cooling is sometimes used to infer an anticlockwise *P–T* path. In compressive settings, the interplay of thickening and heating results in *P–T* paths that are clockwise when tectonic burial is rapid relative to heating, or hairpin in style (with similar prograde and retrograde paths) when the heat transport can maintain an evolving thermal pseudo-equilibrium with slowly changing crust and lithosphere thicknesses (e.g., Copley and Weller 2022; England and Thompson 1984). Additional effects are therefore required for anticlockwise *P–T* paths to be produced in compressional settings.

One possible mechanism involves the addition of magmatic heat, during or preceding thickening (e.g., Collins and Vernon 1991; Faber et al. 2019; Halpin et al. 2007; Harley 1989; Rubenach 1992). However, when inferring this style of *P–T* path, care must be taken to correctly identify the different spatial and temporal patterns of the regional-scale thermal evolution and any additional contact-metamorphic events that are short lived and spatially localised (Annen 2017; Copley, Weller, and Bain 2023; Voll et al. 1991). In this paper, we investigate this issue by examining a region where magmatically driven anticlockwise *P–T* paths have previously been inferred: the Paleoproterozoic Roineabhal terrane in northwest Scotland (Figure 1; Baba 1998, 1999a; Hollis et al. 2006).

Although the Roineabhal terrane forms part of the Lewisian Gneiss Complex, its constituent lithologies and metamorphic conditions are different from the majority of the Complex. The terrane comprises metasedimentary (Leverburgh and Langavat belts) and metaigneous (South Harris Igneous Complex; SHIC) rocks and is interpreted as an accretionary wedge that formed in an arc setting at c. 1.9 Ga (Baba 1997; Fettes et al. 1992; Mason 2015; Mason, Parrish, and Brewer 2004; Whitehouse and Bridgwater 2001). Studies of the region have consistently inferred anticlockwise *P–T* paths featuring a thermal maximum at ultrahigh temperature (UHT) conditions of ~10 kbar and 950°C and a subsequent pressure maximum at granulite-facies conditions of 13 kbar and 900°C (Baba 1998, 1999a; Hollis et al. 2006). Metamorphism is suggested to have occurred at c. 1.91–1.85 Ga, with peak-T conditions driven by magmatism, and peak-P conditions due to collision and thickening (Baba et al. 2012). Figure 1B shows all documented samples that contain evidence for UHT metamorphism (yellow circles). Of importance later in this paper, these exclusively cluster close to a large meta-anorthosite body that is part of the SHIC.

Below, we integrate petrography, phase equilibria modelling and thermal modelling to explore the thermal evolution of the Roineabhal terrane. We focus on the contrast between the regional-scale *P–T* paths and the short-lived contact metamorphic excursion in the aureole of an anorthosite body. We then generalise our results to discuss the situations in which truly magmatically driven anticlockwise *P–T* paths are feasible, and those in which 'joining the dots' between isolated *P–T* points leads to an incorrect interpretation of the *P–T* history of a region.

2 | Geological Setting

The Lewisian Gneiss Complex of northwest Scotland comprises a series of Archean and Paleoproterzoic terranes that were assembled during the Paleoproterozoic (Friend and Kinny 2001). The Complex is exposed in two main areas: a ~30-km-wide coastal strip on the Scottish mainland and on the 200-km-long Outer Hebrides (Na h-Eileanan Siar) island chain (Figure 1A).

The mainland portion of the Complex is dominantly formed of Archean tonalite-trondhjemite-granodiorite gneiss, with numerous felsic–ultramafic enclaves (Kinny and Friend 1997; Miocevich, Copley, and Weller 2022; Peach et al. 1907), and is divided into the northern, central and southern regions based on peak metamorphic grade, with the central region preserving granulite-facies assemblages, compared with amphibolite-facies metamorphic conditions to the north and south (e.g., Peach et al. 1907; Sutton and Watson 1951). The larger, but lesser-studied, Outer Hebridean portion of the Complex is divided into four regions (Kinny, Friend, and Love 2005), comprising from north to south: (1) a thin sliver of Paleoproterozoic plutonic and metasedimentary rocks, termed the Nis (or 'Ness') terrane, which experienced peak amphibolite-facies conditions; (2) a large tract of amphibolite-facies, Archean tonalite-trondhjemite-granodiorite gneiss containing widespread

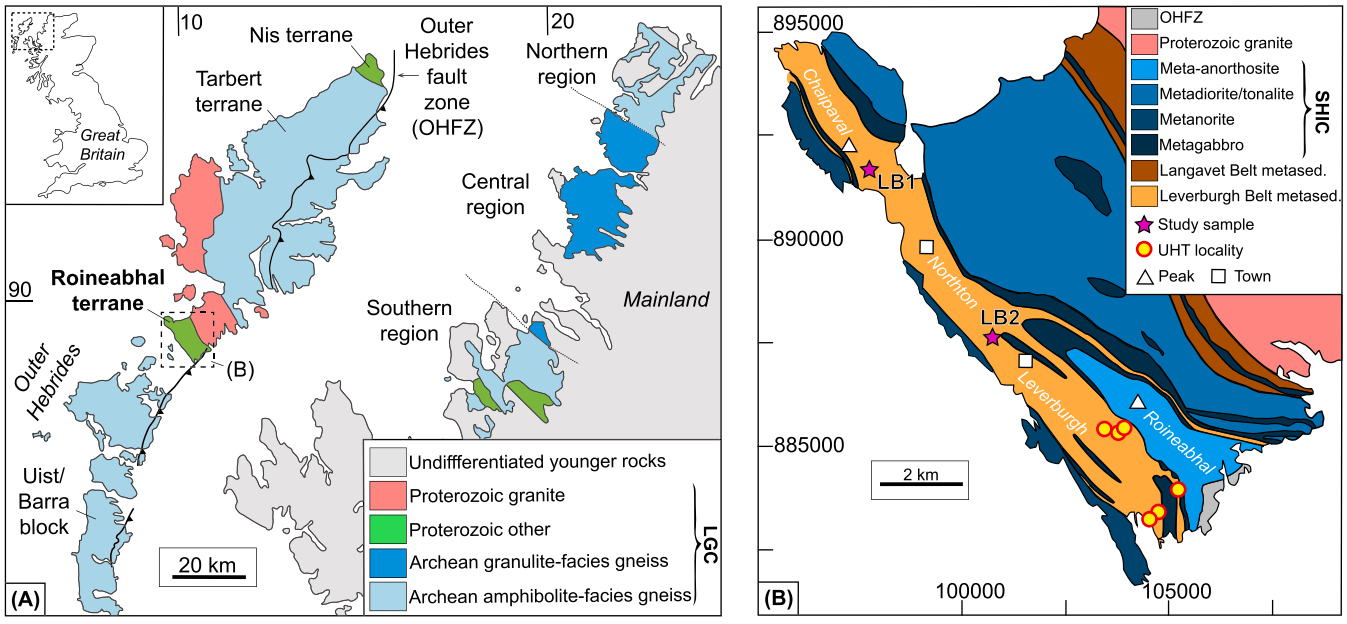

FIGURE 1 | (A) Terrane map of northwest Scotland (adapted from Miocevich, Copley, and Weller 2022). Inset shows location within Great Britain. LGC = Lewisian Gneiss Complex. (B) Geological map of South Harris (adapted from Fettes et al. 1992). SHIC = South Harris Igneous Complex. UHT = ultrahigh temperature.

1675 Ma granite intrusions, known as the Tarbert terrane; (3) a granulite-facies, Paleoproterozoic metasedimentary and metaplutonic complex, known as the Roineabhal terrane (the focus of this study); and (4) an undifferentiated suite of Archean plutonic rocks, known as the Uist/Barra block, which experienced peak granulite-facies conditions (Friend and Kinny 2001). The Proterozoic Nis and Roineabhal terranes are bounded by ductile shear zones and are thought to have been juxtaposed with the Archean units after 1675 Ma, based on their lack of granites of this age (Friend and Kinny 2001). The east-dipping Outer Hebrides fault zone cross-cuts all units along the eastern edge of the Outer Hebrides and has been active as a thrust in Caledonian (and possibly Grenvillian) times and as a normal fault in the Permo-Triassic (Butler, Holdsworth, and Strachan 1995; Imber et al. 2002).

The Roineabhal terrane forms a northwest-trending strip, ~ 8 km wide by 15 km in length, at the southern tip of the Isle of Harris (Na Hearadh; Figure 1A). The terrane comprises three units: the metaigneous South Harris Igneous Complex (SHIC) and the metasedimentary Leverburgh and Langavat belts (Figure 1B). The SHIC intrudes the Leverburgh belt and is tectonically interleaved with the Langavat belt along the sheared eastern terrane boundary, with all units sharing steep deformation fabrics. The Leverburgh belt and SHIC exhibit variably retrogressed high-pressure (~13 kbar), granulite-facies assemblages and are collectively known as the South Harris Granulite Belt, whereas the Langavat belt is thought to have only experienced lower pressure (~6 kbar) amphibolite-facies conditions (Mason 2012) and is not considered further in this paper.

The Leverburgh belt comprises a range of lithologies, including migmatitic pelitic gneiss, psammitic gneiss, mafic gneiss and minor calc-silicate and marble (Baba 1997, 2002). Based on the varied geochemistry of mafic components within the belt (including mid-ocean, ocean-island and arc affinities) and interpreted protoliths of other components (including turbidite, limestone and hemipelagic sediment), the belt is interpreted as an accretionary mélange that formed in an arc setting (Baba 1997, 1999b). The sediments are thought to have been deposited at c. 1.9 Ga based on detrital zircon age populations (Friend and Kinny 2001; Whitehouse and Bridgwater 2001).

The SHIC comprises meta-anorthosite, metanorite, metadiorite, metagabbro and metatonalite. Precise crystallisation ages have been obtained for the norite (1890 +2/−1 Ma; Mason, Parrish, and Brewer 2004), diorite (1888 ± 2; Ma Mason, Parrish, and Brewer 2004) and tonalite (1876 ± 5 Ma; Whitehouse and Bridgwater 2001). U-Pb zircon data from the meta-anorthosite yielded a discordant array on a Concordia diagram, with an upper age intercept of 2491 +31/−27 Ma, and a lower intercept of 1877 +46/−56 Ma, with no obvious relationship between morphology, U content or U/Th ratio (Mason, Parrish, and Brewer 2004). Two interpretations were offered by Mason, Parrish, and Brewer (2004): that the upper and lower intercept represented crystallisation and metamorphism, or inheritance and crystallisation, respectively. Although the former interpretation was initially preferred by Mason, Parrish, and Brewer (2004), due to more recent analysis of field relationships and deformation histories, the 1877 +46/−56 Ma age is now considered to represent the crystallisation age of the anorthosite (Mason 2015), such that the SHIC represents a single period of magmatism. The SHIC has a calk-alkaline chemistry, consistent with formation in an arc setting (Fettes et al. 1992).

Previous studies of the metamorphic history of the region have focused on lithologies from the Leverburgh belt and consistently inferred anticlockwise *P–T* paths featuring a thermal maximum at UHT conditions of ~10 kbar and 950°C and a pressure maximum at granulite-facies conditions of ~13 kbar and 900°C (Baba 1998, 1999a, 2004; Hollis et al. 2006). Figure 1B shows all reported samples that contain evidence for UHT metamorphism (yellow circles), which cluster close to the large meta-anorthosite body that is part of the SHIC. Petrographic observations of aluminosilicate polymorphs indicate that prograde to thermal peak conditions were reached in the sillimanite stability field, peak pressure conditions occurred in the kyanite stability field and the early retrograde evolution occurred back through the sillimanite stability field (Baba 1998). Based on garnet inclusion suites, prograde metamorphic conditions are further constrained to be < 790°C and < 9.5 kbar (Hollis et al. 2006), and via analysis of corona textures, retrograde metamorphic conditions are estimated to be 550°C–650°C and 6.5 ± 1 kbar (Baba 1998, 1999a).

Baba et al. (2012) conducted U–Pb zircon and monazite dating of a range of lithologies from the region and synthesised their data with previous work to suggest that metamorphism occurred over 60 million years at c. 1910–1850 Ma. Burial of the Leverburgh metasedimetary rocks is constrained to have started before 1909 ± 3 Ma, UHT metamorphism initiated by ~1900 Ma, kyanite-grade metamorphism occurred at ~1870 Ma and retrograde assemblages produced during decompression formed at ~1850 Ma. These metamorphic conditions are thought to have occurred in a continuous tectono-thermal event, with the UHT phase driven by advection of heat into the crust by SHIC magmatism, followed by thickening and exhumation in an arc setting (Baba 1997, 1999b).

3 | Petrography

A suite of samples was collected from the region, with two samples from the Leverburgh belt (LB1, LB2) chosen for detailed analysis (pink stars, Figure 1B; locations given in Table S1). These samples were selected because of their potential to constrain different aspects of the prograde, peak and retrograde metamorphism in the region, as well as being located at variable distances from previously documented UHT localities (yellow circles, Figure 1B). The samples are described below and are the subject of phase equilibria modelling in the next section.

3.1 | Analytical Techniques

All analytical measurements were conducted in the Department of Earth Sciences at the University of Cambridge. Full thin section phase maps and mineral abundances were calculated for each study sample by 'quantitative evaluation of minerals by scanning electron microscopy' (QEMSCAN), using a Quanta650F scanning electron microscope. Pixel sizes

varied from 2 to 10 μm depending on the coarseness of the sample. Aluminosilicate polymorphs were confirmed using a LabRam300 Horiba Raman microspectrometer with a 532.05 nm wavelength laser. The laser was focussed on the sample by a 50× magnification objective (numerical aperture = 0.50) and the spot size at the sample surface was ~2 μm in diameter. The laser power was set at the source at 250 mW. The laser wavelength was eliminated by a notch filter and the signal was dispersed using a 600 grooves mm^{-1} grating and analysed by a CCD detector. The spectrometer was calibrated before each session using the 528 cm^{-1} peak of a silicon standard. Mineral compositions were measured by Electron Microprobe Analysis (EMPA) using a Cameca SX100. Analyses were carried out with a 20 kV acceleration voltage, a 2–3 μm beam diameter and a 20 nA probe current. Representative analyses are reported in Tables S2 and S3. Mineral cation totals were calculated using AX (Holland 2009), which calculates mineral compositions based on standard number of oxygens per formula unit and estimates Fe^{3+} based on stoichiometry. All abbreviations follow Whitney and Evans (2010).

3.2 | LB1: Pelitic Migmatite

Sample LB1 was collected from the northwest part of the Leverburgh belt (Figure 1B). In outcrop, the unit exhibits compositional layering between lighter coloured layers dominated by quartz and K-feldspar and darker-coloured layers and clots featuring more abundant garnet, biotite and kyanite (Figure 2A). Consistent with previous interpretations of this lithology, the unit is interpreted as a stromatic migmatite, with the lighter coloured layers representing the leucosome, and the darker coloured regions the melanosome (e.g., Baba 1998). The study sample was collected from a melanosome-dominant region.

In thin section, the sample contains quartz (34 vol.%), biotite (19 vol.%), aluminosilicate (mainly kyanite with some sillimanite, 16 vol.%), garnet (14 vol.%), K-feldspar (14 vol.%) and plagioclase (2 vol.%) with accessory apatite, ilmenite, monazite, pyrite, rutile and zircon (Figure 2B). Matrix biotite and kyanite define a weak foliation sub-parallel to the compositional layering.

Garnet forms subhedral, poikioblastic grains, with quartz, biotite, plagioclase, rutile and sillimanite present as inclusions throughout the grain interiors (Figure 2C,D). Chemical profiles across garnet grains indicate that the core and mantle regions feature flat profiles, whereas the rim regions feature increases in Mn, Ca and Fe and decreases in Mg (Figure S1A,B). These profiles are interpreted to have resulted from diffusive homogenisation at high temperatures, followed by modification during retrograde resorption (Tracy 1982; Caddick, Konopasek, and Thompson 2010). Garnet grains are commonly surrounded by thin films of plagioclase (Figure 2B), or embayed by biotite-quartz symplectite and/or kyanite (Figure 2E). All of these garnet margin features are interpreted as retrograde, with plagioclase rimming garnet typical of decompression following peak conditions, and the replacement of garnet with biotite, quartz and kyanite suggestive of post-peak retrogression following melt crystallisation, as is common in granulite-facies migmatites (e.g., Kriegsman 2001).

Kyanite is present as poikiloblastic grains throughout the matrix, commonly with quartz, biotite and rutile inclusions. The grains feature irregular, embayed margins and show evidence of deformation including undulose extinction and kink bands (Figure 2F; Blereau et al. 2024). Minor sillimanite is also present in the matrix (in addition to inclusions in garnet), occurring as clusters of prismatic needles that occur along grain boundaries, and is interpreted as retrograde due to the fine grain size (Figure 2G). Collectively, and consistent with previous authors, kyanite is interpreted to have been present at peak conditions, with sillimanite stable during prograde and retrograde metamorphism (Baba 1998; Hollis et al. 2006).

K-feldspar exhibits microperthite and microcline textures, and commonly features myrmekite along its margins, which is interpreted as retrograde (Figure 2H). Away from biotite-quartz symplectites, biotite forms abundant laths in the matrix that share grain boundaries with all major phases and is interpreted as part of the peak assemblage. Quartz forms irregular grains with interfingering sutures, suggesting recrystallisation by grain boundary migration. Minor ilmenite is also present as rims on some matrix rutile and is interpreted as retrograde (Figure 2E).

Overall, biotite, garnet, plagioclase, quartz, rutile and sillimanite are interpreted to have been present during prograde metamorphism, with a peak assemblage characterised by garnet, K-feldspar, kyanite, biotite, quartz, rutile and melt. Retrograde effects include: evidence for the replacement of garnet with biotite, quartz and kyanite (likely during melt crystallisation); the development of plagioclase rims on garnet, ilmenite rims on rutile and a transition from kyanite to sillimanite stability (likely during decompression); and evidence for high-temperature deformation. Given the absence of muscovite in the sample, the aluminous pelite bulk composition and the interpreted melt-assisted retrogression products, peak conditions were likely characterised by reaching (but not exceeding) biotite-dehydration melting in the kyanite stability field.

3.3 | LB2: Quartz-Bearing Biotite Amphibolite

Sample LB2 was collected from an amphibolite horizon within the central portion of the Leverburgh belt (Figure 1B). The sample comprises quartz (45 vol.%), plagioclase (28 vol.%), amphibole (17 vol.%) and biotite (9 vol.%), with accessory apatite, calcite, epidote, ilmenite, magnetite, pyrite and titanite. The sample is compositionally layered and features a composite S-C fabric consistent with shear deformation (Figure 3A).

Quartz is present as aggregates of grains forming ribbons (Figure 3B). The grains exhibit undulose extinction and are interpreted to have undergone dynamic recrystallisation. Plagioclase is oligoclase in composition, partially sericitised and present as subhedral porphyroclasts up to ~1 mm, suggesting that significant grain size reduction of the generally finer-grained matrix may have occurred (Figure 3C). Amphibole is present as platy grains up to ~0.5 mm, and as spongy

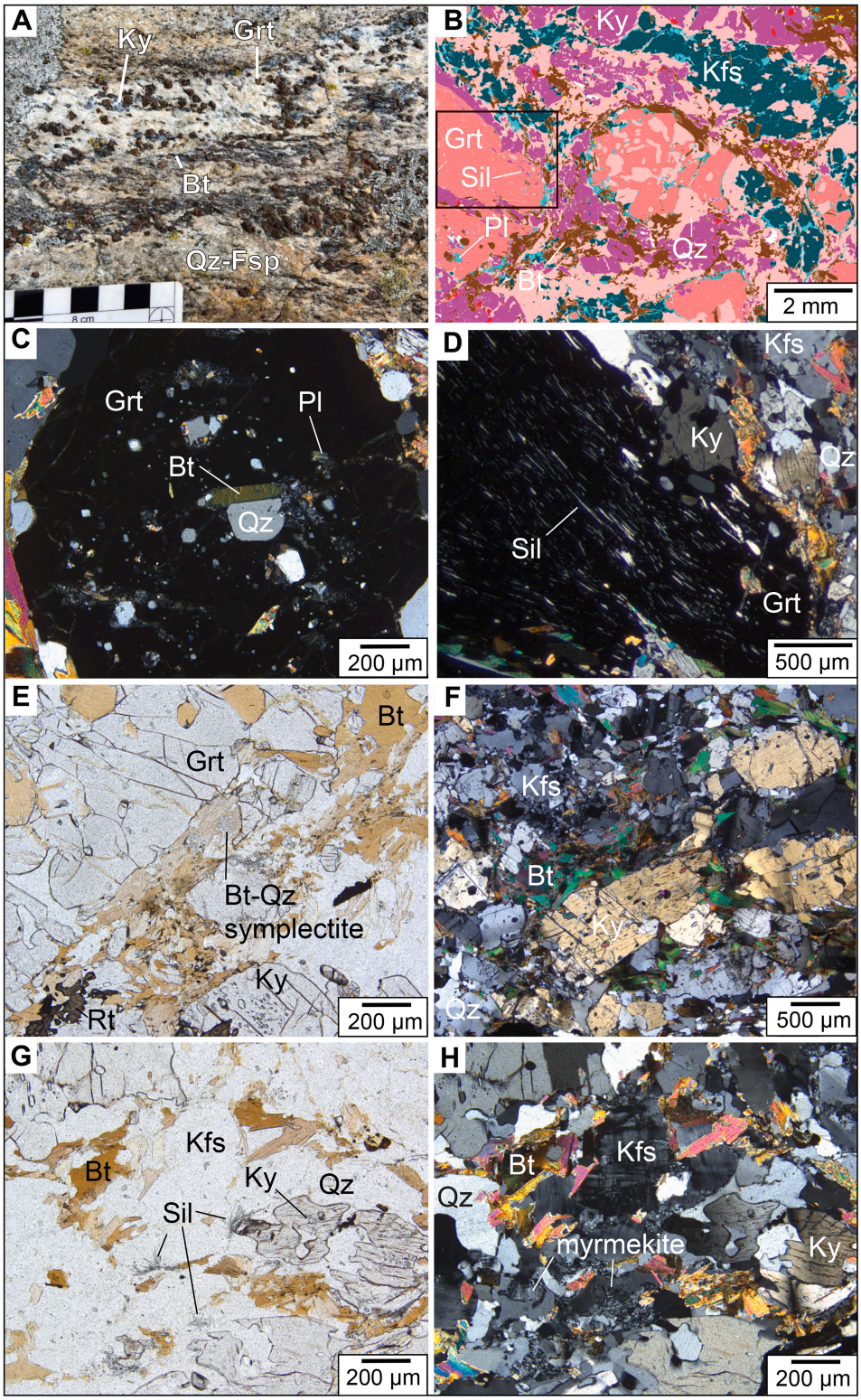

FIGURE 2 | Sample LB1 petrography. (A) Field photo of LB1 outcrop. (B) QEMSCAN image showing the main assemblage of the sample, including thin rims of plagioclase (light blue) around some garnet grains. (C–H) Photomicrographs viewed under crossed polars (C, D, F, H) and plane polarised light (E, G) showing (C) a poikiloblastic garnet grain, (D) the boxed region of the QEMSCAN image (B), highlighting the aligned sillimanite needles, (E) a symplectite formed of biotite and quartz on the margin of a garnet grain, (F) deformed blades of kyanite in the matrix, (G) sillimanite needles in the matrix adjacent to anhedral kyanite blades and (H) myrmekite on the margin of K-feldspar grains.

intergrowths with quartz, and is magnesiohornblende to pargasite in composition (Figure 3D). The spongy amphibole-quartz intergrowths may represent pseudomorphs after clinopyroxene (Ashworth, Birdi, and Emmett 1992). Biotite is present as discrete laths in the matrix, and also on the margins of, and as blebs within, amphibole grains, suggesting that biotite is in part replacing amphibole. Accessory ilmenite is present as inclusions within plagioclase porphyroclasts and is interpreted as relict.

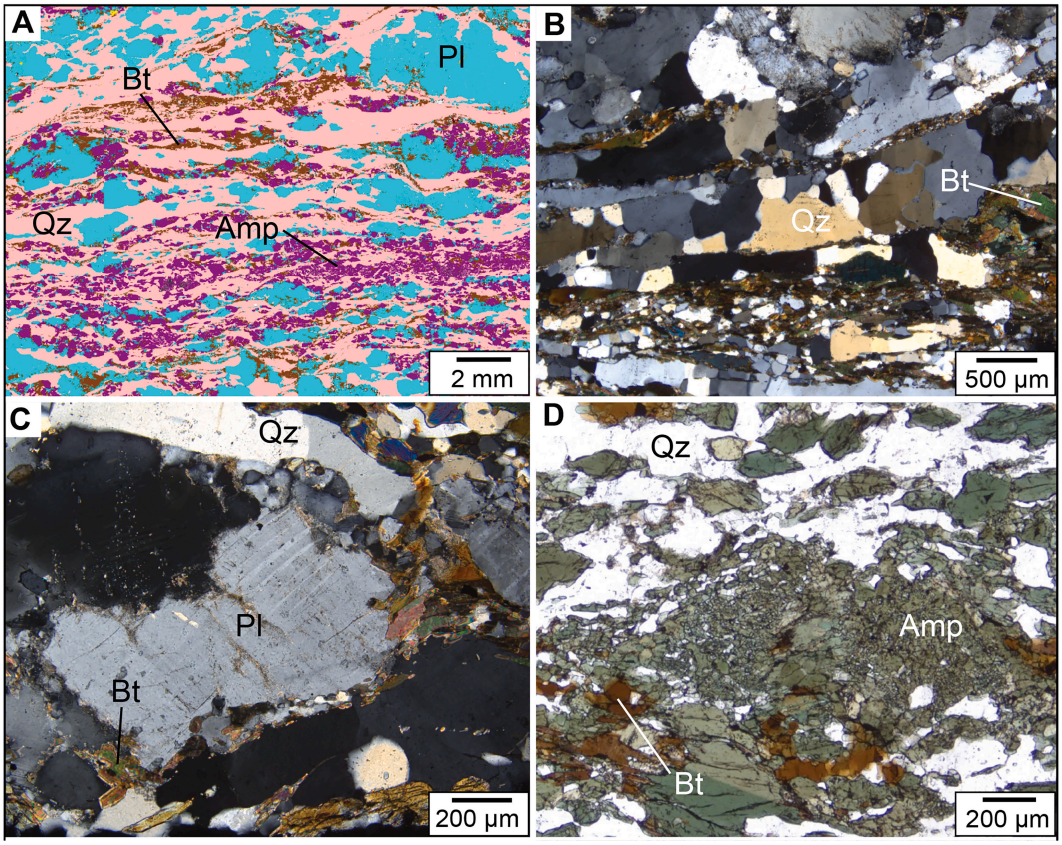

FIGURE 3 | Sample LB2 petrography. (A) QEMSCAN image showing the main assemblage and a weak S-C fabric. (B, C) Photomicrographs viewed under crossed polars showing (B) ribbons of elongate quartz aggregates and (C) sericitised plagioclase grain with small recrystallised grains around the margin. (D) Plane-polarised photomicrograph showing 'platy' amphibole being replaced by biotite and 'spongy' amphibole intergrown with quartz.

Accessory epidote forms on the margins of plagioclase and is interpreted as relatively late. Other accessory phases exhibit no systematic petrographic location.

Overall, sample LB2 is interpreted to have experienced shear deformation in the stability field of quartz, plagioclase, amphibole and biotite ± accessory phases. The observation of epidote and biotite partially replacing plagioclase and hornblende, respectively, suggests that the sample likely approached equilibration down temperature, close to the epidote amphibolite-amphibolite facies boundary, indicating that the preserved assemblage(s) are retrograde in nature. The sample contains no record of granulite-facies metamorphism, although the amphibole-quartz intergrowths potentially represent pseudomorphs after clinopyroxene.

4 | Phase Equilibria Modelling

Pseudosection modelling was applied to both samples (Figure 4A–C) to define the *P–T* conditions of metamorphism. Pseudosections were constructed using THERMOCALC v3.51s (Powell and Holland 1988) with dataset ds62 (Holland and Powell 2011). MAGEMin (Riel et al. 2022) was used for melt reintegration calculations (see below and Figure S2). Calculations for felsic sample LB1 were carried out in the $MnO–Na_2O–CaO–K_2O–FeO-MgO–Al_2O_3–SiO_2–H_2O–Ti_2O–O_2$ (MnNCKFMASHTO) model system using the activity–composition (*a–x*) relations described in White et al. (2014), with the updated 4TR feldspar model of Holland, Green, and Powell (2022). Calculations for mafic sample LB2 were carried out in the Mn-free, NCKFMASHTO model system using the *a–x* relations of Green et al. (2016), including the low-temperature 'omphacite' clinopyroxene model, with the updated 4TR feldspar model of Holland, Green, and Powell (2022). Quartz, rutile, kyanite, sillimanite, titanite and H_2O were modelled as pure phases. Model bulk compositions were calculated by combining QEMSCAN-derived phase vol.%, with EMPA-derived phase composition measurements. Where mineral zoning was observed (e.g., Figure S1), spherical averaging of the grains was used to determine average compositions. All model bulk compositions are provided in Table S4. Water contents for each sample were chosen depending on the metamorphic stage being modelled, as detailed below.

4.1 | LB1 Peak Conditions

Figure 4A shows a *P–T* pseudosection for sample LB1, calculated using the observed water content. The interpreted peak assemblage field (red text) occurs at 800°C–870°C and 10–15 kbar. The water-unsaturated solidus forms the low-T boundary to the peak field, consistent with the view that migmatites typically re-equilibrate at the solidus as defined by the retained melt, thus water content, of the sample (White, Powell, and Halpin 2004). Compatible with this interpretation, the

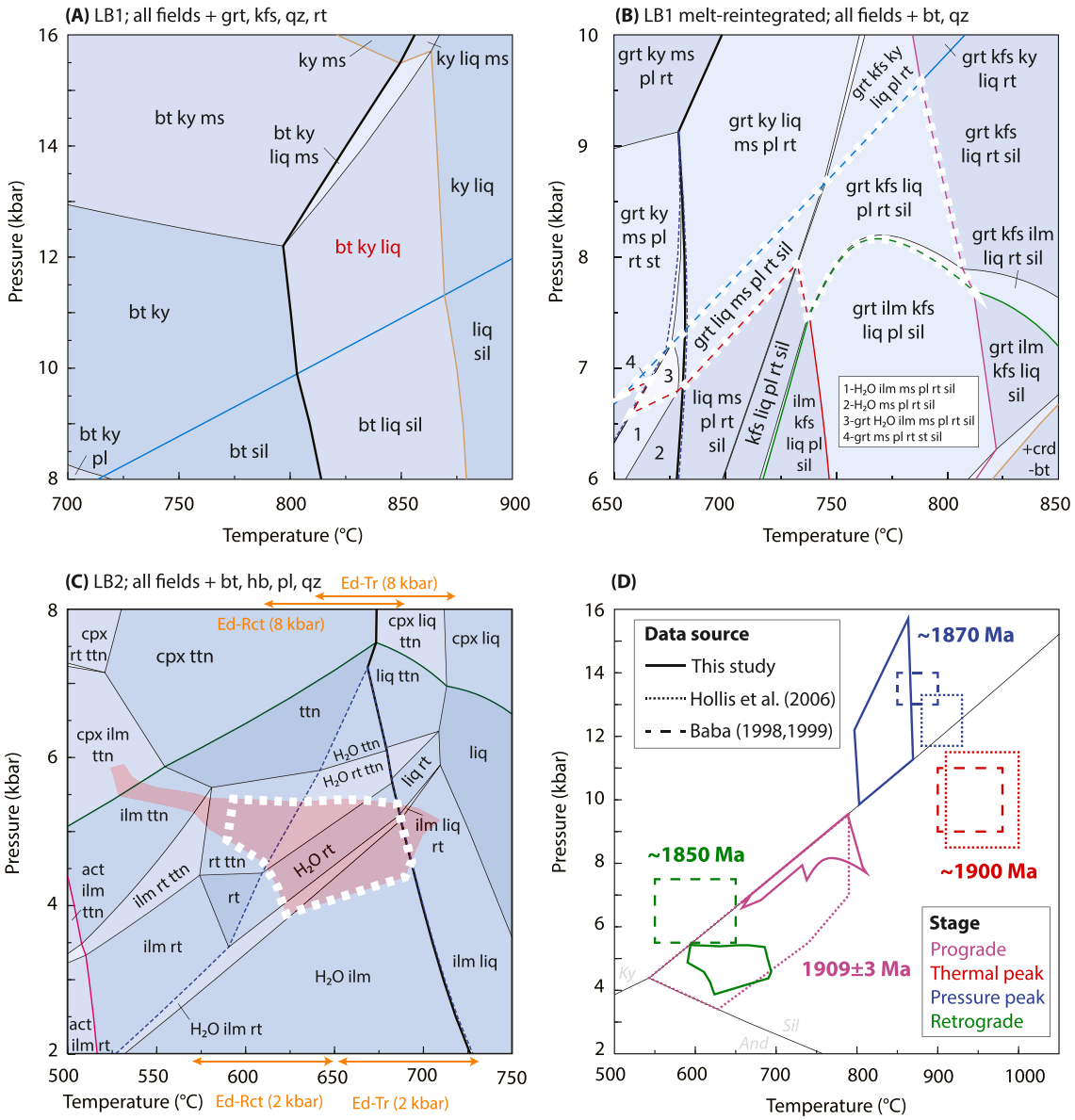

FIGURE 4 | Phase equilibria modelling. (A) LB1 *P–T* pseudosection. The observed peak assemblage field is highlighted by red text. Zero-mode isolines highlighted for liquid (thick), biotite (brown) and kyanite-sillimanite (blue). (B) LB1 melt reintegrated *P–T* pseudosection. Zero-mode isolines highlighted as (A) plus for H_2O (dashed blue), garnet (red), rutile (green) and plagioclase (purple). Dashed white polygon highlights garnet inclusion suite. (C) LB2 *P–T* pseudosection. Zero-mode isolines highlighted for liquid (thick), H_2O (dashed blue), actinolite (red) and clinopyroxene (green). Shaded red area shows where all major phases are within ±1 mode% of the QEMSCAN-derived phase proportions (Figure S3). Dashed white polygon highlights where all constraints are met; see text for discussion. (D) *P–T* constraints with associated ages from Baba et al. (2012).

model also predicts an increase in biotite, quartz and kyanite mode, and a decrease in garnet mode, on a down-T approach to the solidus, in agreement with retrograde reactions inferred from petrographic observations. To higher temperatures, biotite is lost from the assemblage. Owing to observations of equant biotite grains sharing straight grain boundaries with other peak phases (Figure 2), complete biotite breakdown is interpreted not to have been exceeded, such that 870°C represents an upper limit for this sample. Overall, the peak field is consistent with the interpretation of the sample having reached, but not exceeded, biotite-dehydration melting. The *P–T* conditions overlap with, and extend to slightly lower T, previous estimates for the peak-P conditions in the region (Figure 4D; Baba 1998, 1999a; Hollis et al. 2006).

4.2 | LB1 Prograde Conditions

The garnet inclusion suite in sample LB1 (biotite, quartz, plagioclase, sillimanite and rutile) provides a window into the prograde history. To interpret this assemblage, a new pseudosection is required that incorporates a melt reintegration correction, because the preservation of granulite-facies assemblages suggests that some melt has been lost from the sample (White, Powell, and Clarke 2002). We apply a stepwise melt reintegration approach, integrating successive batches of 7 modal% (~vol.%) melt in equilibrium with the 9 kbar water-undersaturated solidi until the 9 kbar water-saturated solidus is reached. This approach reverses sporadic melt loss during burial, using the 7 vol.% melt connectivity transition of Rosenberg and Handy (2005), and

required three steps and 15 modal% melt to be reintegrated; a total that is consistent with expected melt volumes from a sample that reached (but did not exceed) biotite-dehydration melting (White, Powell, and Holland 2001). The intermediate pseudosections are provided in Figure S2, with the final melt-reintegrated pseudosection shown in Figure 4B. The garnet inclusion suite (dashed white polygon, Figure 4B) is stable over conditions of 6.5–9.5 kbar and 650°C–800°C, yielding a prograde constraint that is consistent with previous estimates (Figure 4D; Hollis et al. 2006).

4.3 | LB2 Retrograde Conditions

Figure 4C shows a *P–T* pseudosection for sample LB2 calculated using the observed water content. The major assemblage in this sample, which is > 99 vol.% quartz, plagioclase, hornblende and biotite, is present across all fields. Accessory phases are not used to further constrain *P–T* conditions as the presence or absence of small-volume phases contribute very little to the overall Gibbs free energy of the assemblage, demanding implausible precision from the thermodynamic models (Weller et al. 2024), and are highly sensitive to relatively poorly constrained parameters, such as the proportion of ferrous to ferric iron (Diener and Powell 2010). Rather, three other constraints are applied. First, the absence of melt (thick line), clinopyroxene (green) and actinolite (red) implies *P–T* conditions of < 7.5 kbar and ~500°C–700°C. Second, the hornblende-plagioclase thermometer of Holland and Blundy (1994) was applied to five pairs of adjacent hornblende-plagioclase grains. At 5 kbar, temperatures ranged from 675°C to 696°C for the edenite-tremolite calibration and 610°C–652°C for the edenite-richterite calibration. Given the limited spread in temperatures, the average of all data are used, yielding 686 ± 40 °C for edenite-tremolite and 631 ± 40°C for edenite-richterite (at 5 kbar; the P sensitivity of this thermometer is shown on Figure 4C). Third, the modes of the major phases vary across the modelled *P–T* region (Figure S3), with the red shaded region highlighting where the modes are within ±1% of the observed proportions. All of these constraints are satisfied in the white dashed region on Figure 4C at ~5 kbar and 650°C, which we interpret as being on the sample's retrograde path based on the petrological observations outlined above. This estimate is slightly lower pressure than previous retrograde estimates (Figure 4D; Baba 1998, 1999a), but is consistent with retrograde conditions passing through sillimanite stability, as suggested by this and previous studies (Baba 1998; Hollis et al. 2006).

5 | The Thermal Evolution of South Harris

Previous studies have suggested South Harris experienced an anticlockwise *P–T* path with an initial phase of UHT metamorphism driven by magmatism followed by higher-P granulite-facies metamorphism due to collision and thickening (e.g., Baba 1999a; Hollis et al. 2006). However, it is important to address whether intrusions in the region can result in a true anticlockwise *P–T* path, in which conditions transitioned directly from peak-T to peak-P conditions, or whether they represent a short-lived thermal pulse superimposed on a more generic *P–T* path. We first present some scaling arguments, which are applicable to all regions undergoing thickening and intrusion, to consider what magmatic intrusion characteristics would be compatible with producing anticlockwise *P–T* paths (Figure 5). We then present an example thermal model that is consistent with all the observations discussed above (Figure 6), which is specific to South Harris. Finally, we discuss the implications of our results for previously documented anticlockwise *P–T* paths.

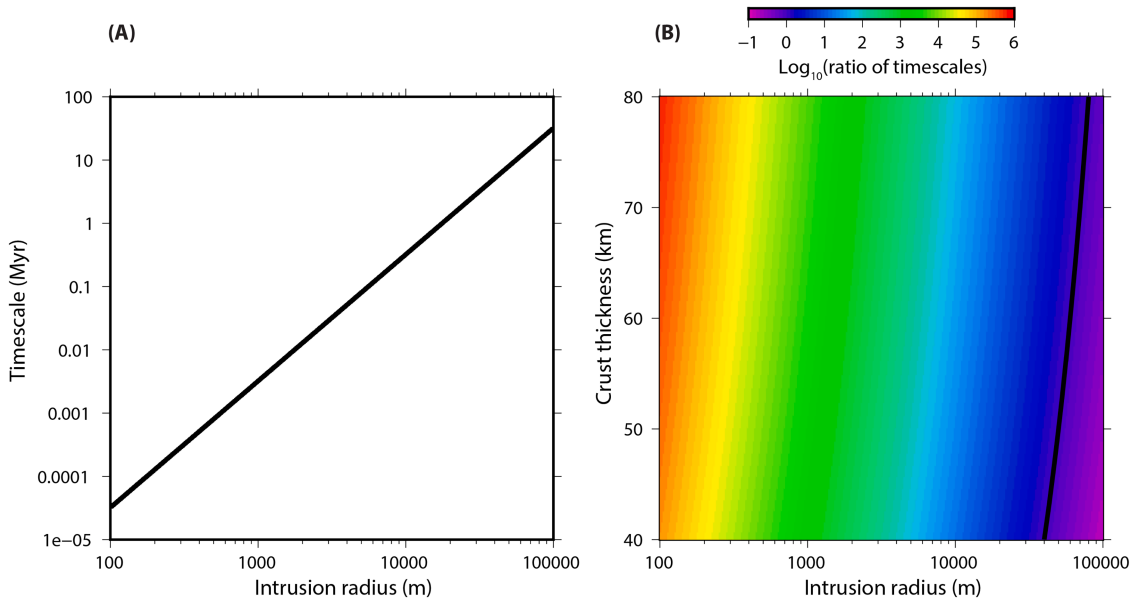

FIGURE 5 | (A) The timescale for cooling of an intrusive body, which is also the regularity of repeated intrusions of a given size that would be required to prevent cooling in the interim. (B) Ratio of the timescale of diffusive thermal equilibration through the crust to that of heating from intrusion. The thick black line is where they are equal.

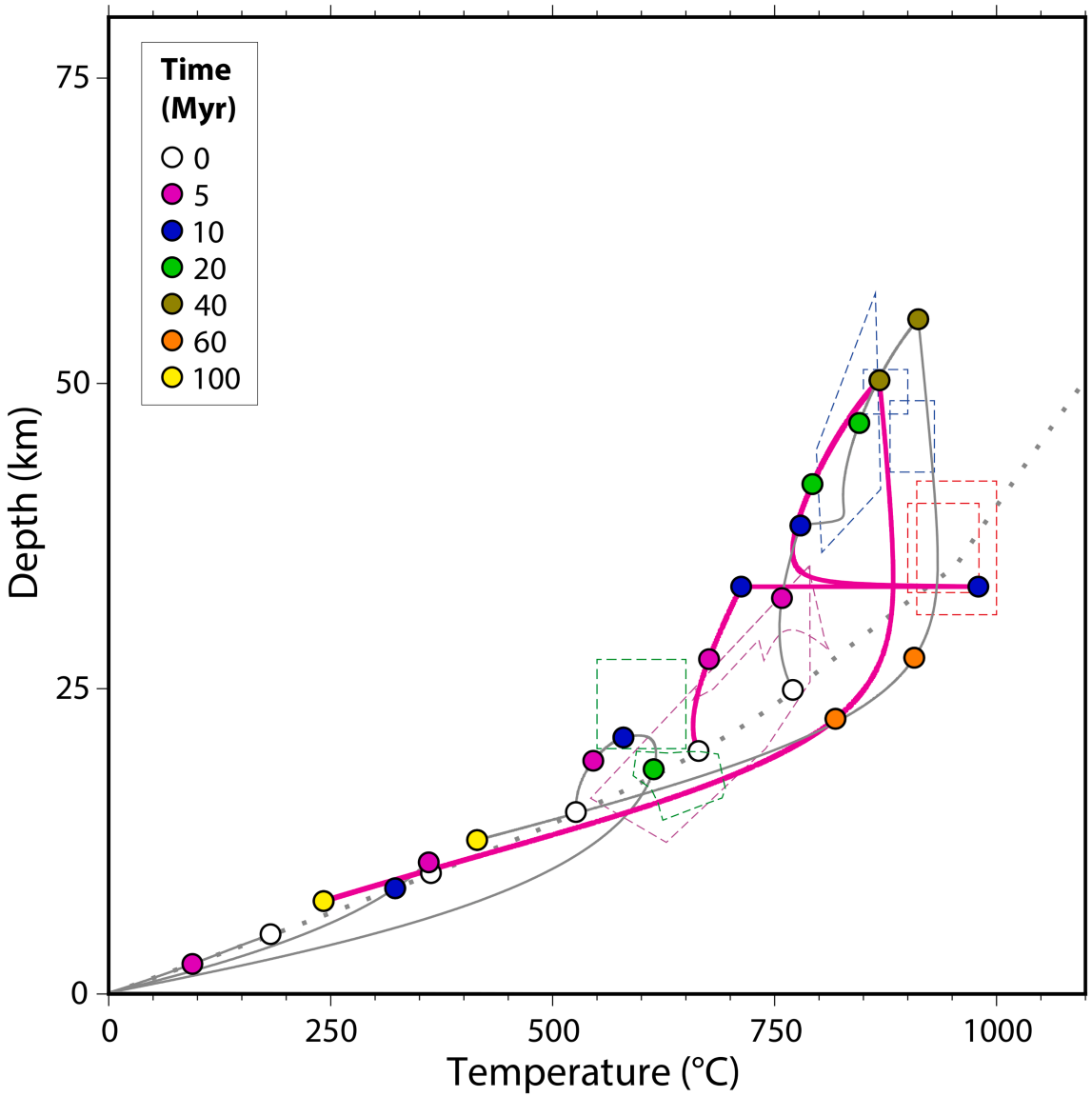

FIGURE 6 | Thermal model result. The dotted grey line shows the initial geotherm, solid lines track rocks initially located at 5 km depth intervals within the sedimentary pile, coloured circles indicate times since the start of the model run, and the background dashed polygons are the *P–T* constraints from Figure 4D. One *P–T* loop is highlighted in pink, which represents the approximate structural level of South Harris; see text for discussion.

5.1 | Scaling of Thermal Timescales

Timescales of regional metamorphism are governed by the interplay of thickening, erosion, radiogenic heating and the thicknesses of the crust and the mantle lithosphere (England and Thompson 1984; Copley and Weller 2022) and are commonly 10s Myr in duration. Consistent with this timescale, regional metamorphism on South Harris has been documented to have occurred over ~60 Myr (Figure 4D).

The characteristic thermal timescale for diffusive cooling of an intrusion (τ), and so heating of the surroundings, depends upon the size of that intrusion, as:

$$\tau = l^2/(\pi^2\kappa) \quad (1)$$

where l is the characteristic lengthscale and κ is the thermal diffusivity ($\sim 10^{-6}$ m^2/s in common rock types). Figure 5A shows the relationship between τ and l, and Figure 5B compares the ratio of timescales for thermal equilibration of thickened crust (using the expression given above, with l now representing the crustal thickness) versus cooling of an intrusion. For magmatically driven anticlockwise *P–T* paths to occur, comparable timescales of magmatic heat input and crust-scale re-equilibration are required (i.e., black line, Figure 5B). Figure 5B shows the case for a single intrusion, and in this case, intrusions tens of kilometres in size would be required to provide the necessary duration of heating to generate an anticlockwise *P–T* path.

Alternatively, igneous heating could instead be achieved by the repeated injection of smaller intrusions. In this situation, the intrusions would need to occur separated by durations of less than τ (Figure 5A), otherwise the surrounding crust would cool in the time between intrusions. For example, 1 km radius intrusions would need to occur with regularity on the order of every 10^3 yr. If such intrusions instead occurred more widely spaced in time, the resulting *P–T* paths would represent multiple

short-timescale excursions from a regional *P–T* path, rather than an anticlockwise *P–T* path.

Field relations in South Harris show that the heat source for UHT metamorphism was the anorthosite intrusion. All documented UHT samples (yellow circles, Figure 1B) are clustered around this intrusion, indicating a contact metamorphic origin for the heat. Widespread thermal peak biotite-bearing assemblages occur away from the intrusion (e.g., LB1), indicating that UHT conditions were not attained anywhere outside of the thermal aureole of the anorthosite. As field relations indicate that UHT metamorphism was only related to the anorthosite, the implication is that its intrusion temperature was higher than those of the other magmatic components of the SHIC, consistent with the observation of UHT metamorphism in numerous other anorthosite contact aureoles (e.g., Areback and Andersson 2002; Blereau et al. 2017). If l is taken as 2–6 km (the dimensions of the anorthosite), then τ is in the range 10–150 kyr (Figure 5A). This timescale is orders of magnitude shorter than those associated with regional-scale *P–T* loops, including the ~60 Myr implied by previous dating in South Harris.

When applied to South Harris, the above scaling arguments demonstrate that on a diagram of *P–T* conditions, the UHT metamorphism should not be joined directly to the granulite-facies regional metamorphism to form an anticlockwise *P–T* path, as the two processes have distinct spatial and temporal characteristics. Taken as a region, prograde and retrograde regional metamorphism can be seen to have sampled similar parts of *P–T* space, resulting in a narrow 'hairpin' regional *P–T* loop, with a peak at ~800°C–900°C and 10–15 kbar (Figure 4D). Superimposed upon this history is a short-lived thermal excursion to UHT conditions. The timescale of diffusion between this intrusion and the surroundings, compared to the regional metamorphic timescale, shows that the heating and cooling would have been close to isobaric (because there would have been insufficient time for much simultaneous thickening to occur), and the *P–T* conditions would have returned to close to the pre-intrusion values, on the hairpin *P–T* loop.

5.2 | Numerical Model

Although the above concept can be demonstrated with the simple scaling arguments described there, to further illustrate the metamorphic history of South Harris we have produced a numerical thermal model (Figure 6) constructed using the method of Copley and Weller (2022). The limited available observational constraints make this thermal model a non-unique fit to the observations. However, our purpose here is to demonstrate that likely values of the model parameters result in a thermal model that illustrates the scaling arguments presented above and reproduces the observations from South Harris.

Based upon previous suggestions for the geological history of the region (Baba 1997, 1999b), we model the thickening of a sediment pile (i.e., an accretionary wedge) above underthrusting oceanic crust and mantle. In a reference frame attached to the thickening layer, and with minimal lateral variations in the underthrusting material, we can adequately model the temperature structure in one dimension (Copley and Weller 2022; England and Thompson 1984). The oceanic crust is modelled as a layer 10 km thick (to account for a possible higher mantle potential temperature at the time, e.g., Weller et al. 2019; changes to this value do not significantly affect the model results), above 40 km thickness of lithospheric mantle. The total lithosphere thickness could plausibly be anywhere in the range 0–100 km, depending upon the age of the oceanic lithosphere at the time of underthusting, and the value used here is chosen to match the observations and to be well within the possible range. The model starts with a sedimentary pile with a thickness of 25 km. This choice is based upon the metamorphic conditions recorded by metasedimentary rocks in the earliest recorded part of the *P–T* path. There was presumably some thickening before that which we model here, in order to achieve this thickness of sediment. However, given that no information is available regarding the initial geometry and early history of the sedimentary sequence, including when and how any early thickening occurred, we instead start our model with a situation that is consistent with the first piece of *P–T* information we have available.

In the model, the oceanic crust and mantle have no radiogenic heating, based upon previously suggested values being too low to play a significant role in the model behaviour (Hasterok et al. 2018). The sediment pile is modelled as having a radiogenic heating rate of 2.1 $\mu W/m^3$, based upon values measured for relevant sedimentary rocks (Hasterok et al. 2018). Where rocks reach temperatures above a likely water-saturated pelite solidus value (650°C), the radiogenic heating is re-distributed evenly throughout the overlying rocks that are at temperatures below the solidus, to approximate the transport of heat-producing elements by melts. The sediment pile thickens at a rate of 2.4 mm/yr (chosen to fit the observations from South Harris), for 40 Myr (based upon the dating results from South Harris discussed above), and the erosion coefficient (Copley and Weller 2022) is 1.5 /s (also chosen to fit the observations from South Harris). At 10 Myr (based upon the dating results from South Harris discussed above), a 2-km-thick igneous body (the width of the SHIC anorthosite) is emplaced at a temperature of 1100°C (the anorthosite liquidus; Bohlen and Essene 1978) at a depth of 33 km.

The dotted grey line on Figure 6 shows the initial geotherm, and other geotherms can be inferred from connecting coloured circles of equal ages. The lines track rocks initially located at 5 km depth intervals from 5 to 25 km (i.e., within the sedimentary pile), with the deepest point representing the sediment-basement interface. The coloured circles indicate times since the start of the model run. The corner in the depth-temperature-time paths indicates the end of thickening at 40 Myr, at which point erosion then dominates the vertical motions, as the thickened crust continues to increase in temperature. For points located in the lower parts of the sedimentary pile, the model reproduces the *P–T* conditions from the Rhoinebhal terrane (background dashed polygons, Figure 6), and their relative timing (Figure 4D), and features a short-timescale and spatially localised excursion to UHT conditions superimposed on a generic pattern of clockwise *P–T* loops. One *P–T* loop is highlighted in pink, which passes through prograde, thermal peak, pressure peak and retrograde conditions that resemble those from South Harris, and could be considered to roughly approximate the structural level now exposed at the surface there. We note that the detailed geometry of the retrograde

path is not well constrained and in the model depends upon the erosion law used (Copley and Weller 2022). Plausible erosion laws result in models that pass through the observed retrograde conditions, as the pre-thickening geotherm is re-approached following erosion and cooling, but the *P–T* trajectory between the pressure-peak and these conditions would require additional observational information to constrain.

Figure 6 is not unique in being able to match the observations, which are insufficient to uniquely define all parameters for a single successful model (such as the thickening rate, erosion coefficient and lithosphere thickness), which is therefore not our purpose. However, the model illustrates the concept explained using scaling arguments above and demonstrates that using a combination of parameters that can be independently estimated, and plausible suggestions for those than cannot, can reproduce the observations from South Harris. The model also demonstrates the dangers of simply extrapolating between peak-*T* and peak-*P* conditions to infer anticlockwise *P–T* paths. Owing to the water content of mineral assemblages typically decreasing with increasing temperature, it is unlikely that rocks will maintain equilibrium between a contact-metamorphic thermal peak and a subsequent regional-metamorphic pressure peak (Guiraud et al. 2001). Therefore, in the absence of petrographic constraints, the thermal viability of proposed anticlockwise *P–T* paths needs to be critically assessed.

5.3 | Implications for Previously Documented Anticlockwise *P–T* Paths

Given the scaling arguments presented in this study, magmatically driven anticlockwise *P–T* paths are likely to be rarer than reported, regardless of whether proposed to be occurring at high pressures as in this study and others (e.g., Faber et al. 2019), or lower pressures as in other regions (e.g., Rubenach 1992). Instead, many paths are more likely to have the form shown by the pink line in Figure 6, due to the frequently longer timescales of crustal thickening versus magmatic heat input.

The above arguments are focused on the intrusion of a discrete igneous body during thickening. A common class of documented anticlockwise *P–T* paths involve isobaric cooling from peak conditions, such as documented in numerous (often Proterozoic) granulite belts (Bohlen and Mezger 1989; Halpin et al. 2007; Harley 1989; Santosh and Sajeev 2006). These *P–T* paths are often attributed to thickening accompanied by, or preceded by, large volumes of magmatic accretion, either above or surrounding the sample that records the subsequent isobaric cooling (Wells 1980). The scaling arguments presented above show that for such a signal to be a long-term *P–T* trajectory, rather than a brief excursion due to the input of magmatic heat at close to peak-*P* conditions, requires large volumes of magmatic addition, of up to tens of kilometres in thickness. Twin implications of this finding are that: (1) where long-duration isobaric cooling has been inferred as part of a *P–T* path, a large volume of igneous activity can be inferred (possibly later lost to erosion on exhumation of the structural level that experienced isobaric cooling); and (2) such a situation is likely to be unusual in modern-style mountain belts in continent-continent collision zones, due to the volumes of magmatism being insufficient (e.g., Cao et al. 2022). Isobaric cooling could therefore be taken as diagnostic of mountain belts with a significant input of subduction-related magmatism (e.g., Will and Schmadicke 2003), such as the Andes at the present day (where up to 40% of the thickening beneath the volcanic arc is thought to be due to magmatic addition; Lamb and Hoke 1997), or of metamorphism under a melt-rich thermal regime early in Earth's history. However, we emphasise that such an inference is only possible if the duration of isobaric cooling can be constrained to be longer than the short-lived cooling during the thermal excursion associated with a single generically sized intrusion emplaced near peak-*P* conditions (e.g., similar to the pink curve on Figure 6, but with the contact-metamorphic high-*T* peak occurring near the high-*P* part of the *P–T* path at 40 Myr).

Finally, we emphasise that without evidence for extremely large volumes of igneous intrusion, or documented timescales of isobaric cooling on the order of millions of years that allow such intrusions to be inferred, it is inadvisable to 'join the dots' of fragmentary points on a *P–T* path to infer a long-term anticlockwise *P–T* loop. Such a decision is likely to obscure the spatially and temporally varying signatures of different drivers of metamorphism (i.e., thickening and intrusion), and so deduce a physically unviable view of the geological evolution of a region.

6 | Conclusions

Phase equilibria modelling of two samples from South Harris yields *P–T* results consistent with previous work in the region, which collectively feature evidence for UHT metamorphism proximal to an anorthosite intrusion, and regional kyanite-grade granulite-facies metamorphism. Scaling arguments and thermal modelling of these results, combined with reported ages of metamorphism, shows that the UHT metamorphism is contact in nature and should not be joined directly to the kyanite-grade granulite-facies regional metamorphism to form an anticlockwise *P–T* path. Rather, the two processes have distinct spatial and temporal characteristics, with the regional metamorphism featuring 'hairpin' *P–T* loops, with a short-lived excursion to high temperatures in the contact aureole of the anorthosite. As rocks undergoing anticlockwise *P–T* paths would typically require hydration to maintain equilibrium along the path, such situations are predisposed to yielding fragmentary *P–T* results. Therefore, it is critical to assess the thermal viability of extrapolation in these instances, with the implication from this study being that anticlockwise *P–T* paths are likely to be rarer than reported.

Acknowledgements

This work was partly supported by Future Leaders Fellowship MR/V02292X/1 (O.W.) and NERC grant NE/W00562X/1 (A.C.). Toba Copley-Williams is thanked for his assistance in the production of Figure 6. We thank Eleanore Blereau and Dave Waters for insightful reviews and Richard White and Johann Diener for editorial input and handling.

Conflicts of Interest

The authors declare no conflicts of interest.

References

Annen, C. 2017. "Factors Affecting the Thickness of Thermal Aureoles." *Frontiers in Earth Science* 5: 82.

Areback, H., and U. Andersson. 2002. "Granulite-Facies Contact Metamorphism Around the Hakefiorden Norite-Anorthosite Complex, SW Sweden." *Norwegian Journal of Geology* 82: 29–44.

Ashworth, J. R., J. J. Birdi, and T. F. Emmett. 1992. "Diffusion in Coronas Around Clinopyroxene: Modelling With Local Equilibrium and Steady State, and a Non-Steady-State Modification to Account for Zoned Actinolite-Hornblende." *Contributions to Mineralogy and Petrology* 109: 307–325.

Baba, S. 1997. "Geology and Geochemical Characteristics of the LEVERBURGH BELt in South Harris, Outer Hebrides, Northwest Scotland." *Journal of Geosciences, Osaka City University* 40: 119–143.

Baba, S. 1998. "Proterozoic Anticlockwise P-T Path of the Lewisian Complex of South Harris, Outer Hebrides, NW Scotland." *Journal of Metamorphic Geology* 16: 819–841.

Baba, S. 1999a. "Sapphirine-Bearing Orthopyroxene-Kyanite/Sillimanite Granulites From South Harris, NW Scotland: Evidence for Proterozoic UHT Metamorphism in the Lewisian." *Contributions to Mineralogy and Petrology* 136: 33–47.

Baba, S. 1999b. "Evolution of the Lewisian Complex in South Harris, Northwest Scotland, and Its Relation to the North Atlantic Craton in the Palaeoproterozoic (2.0 GA)." *Journal of Geosciences, Osaka City University* 42: 115–125.

Baba, S. 2002. "Tectono-Metamorphic Events in the North Atlantic Region in the Palaeoproterozoic From the View Point of High-Grade Metamorphic Rocks in the Lewisian Complex, South Harris, NW Scotland." *Gondwana Research* 5: 757–770.

Baba, S. 2004. "Paleoproterozoic UHT Metamorphism in the Lewisian Complex and North Atlantic Region." *Journal of Mineralogical and Petrological Sciences* 99: 202–212.

Baba, S., D. Dunkley, T. Hokada, K. Horie, K. Suzuki, and K. Shiraishi. 2012. "New Shrimp U-Pb Zircon Ages and Chime Monazite Ages From South Harris Granulites, Lewisian Complex, NW Scotland: Implications for Two Stages of Zircon Formation During Palaeoproterozoic UHT Metamorphism." *Precambrian Research* 200-203: 104–128.

Blereau, E., T. E. Johnson, C. Clark, R. J. M. Taylor, P. D. Kinny, and M. Hand. 2017. "Reappraising the P-T Evolution of the Rogaland-Vest Agder Sector, Southwestern Norway." *Geoscience Frontiers* 8, no. 1: 1–14. https://www.sciencedirect.com/science/article/pii/S1674987116300810.

Blereau, E., S. Piazolo, P. Trimby, and E. Skrzypek. 2024. "Kyanite Microstructural and Microchemical Characteristics Reveal Differences in Growth, Deformation and Chemical Modification: A Case Study From the Paleoproterozoic Suture Zone of South Harris, NW Scotland." *Lithos* 484-485: 107748. https://www.sciencedirect.com/science/article/pii/S0024493724002615.

Bohlen, S., and E. Essene. 1978. "Igneous Pyroxenes From Metamorphosed Anorthosite Massifs." *Contributions to Mineralogy and Petrology* 65: 433–442.

Bohlen, S. R., and K. Mezger. 1989. "Origin of Granulite Terranes and the Formation of the Lowermost Continental Crust." *Science* 244: 326–329.

Butler, C. A., R. E. Holdsworth, and R. A. Strachan. 1995. "Evidence for Caledonian Sinistral Strike-Slip Motion and Associated Fault Zone Weakening, Outer Hebrides Fault Zone, NW Scotland." *Journal of the Geological Society* 152: 743–746.

Caddick, M., J. Konopasek, and A. Thompson. 2010. "Preservation of Garnet Growth Zoning and the Duration of Prograde Metamorphism." *Journal of Petrology* 51: 2327–2347.

Cao, H.-W., Q.-M. Pei, M. Santosh, et al. 2022. "Himalayan Leucogranites: A Review of Geochemical and Isotopic Characteristics, Timing of Formation, Genesis, and Rare Metal Mineralization." *Earth-Science Reviews* 234: 104229. https://www.sciencedirect.com/science/article/pii/S0012825222003130.

Collins, W., and R. Vernon. 1991. "Orogeny Associated With Anticlockwise P-T-T Paths: Evidence From Low-P, High-T Metamorphic Terranes in the Arunta Inlier, Central Australia." *Geology* 19: 835–838.

Copley, A., and O. Weller. 2022. "The Controls on the Thermal Evolution of Continental Mountain Ranges." *Journal of Metamorphic Geology* 40, no. 7: 1235–1270. https://onlinelibrary.wiley.com/doi/abs/10.1111/jmg.12664.

Copley, A., O. M. Weller, and H. Bain. 2023. "Diapirs of Crystal-Rich Slurry Explain Granite Emplacement Temperature and Duration." *Scientific Reports* 13: 13730.

Diener, J. F. A., and R. Powell. 2010. "Influence of Ferric Iron on the Stability of Mineral Assemblages." *Journal of Metamorphic Geology* 28, no. 6: 599–613. https://onlinelibrary.wiley.com/doi/abs/10.1111/j.1525-1314.2010.00880.x.

England, P. C., and A. B. Thompson. 1984. "Pressure-Temperature-Time Paths of Regional Metamorphism I. Heat Transfer During the Evolution of Regions of Thickened Continental Crust." *Journal of Petrology* 25: 894–928.

Faber, C., H. Stünitz, D. Gasser, et al. 2019. "Anticlockwise Metamorphic Pressure–Temperature Paths and Nappe Stacking in the Reisa Nappe Complex in the Scandinavian Caledonides, Northern Norway: Evidence for Weakening of Lower Continental Crust Before and During Continental Collision." *Solid Earth* 10, no. 1: 117–148. https://se.copernicus.org/articles/10/117/2019/.

Fettes, D., J. Mendum, D. Smith, and J. Watson. 1992. "Geology of the Outer Hebrides; Memoir for 1:100 000 (Solid Edition) Geological Sheets, Lewis and Harris, Uist and Barra (Scotland)." British Geological Survey.

Friend, C., and P. Kinny. 2001. "A Reappraisal of the Lewisian Gneiss Complex: Geochronological Evidence for Its Tectonic Assembly From Disparate Terranes in the Proterozoic." *Contributions to Mineralogy and Petrology* 142: 198–218.

Green, E. C. R., R. W. White, J. F. A. Diener, R. Powell, T. J. B. Holland, and R. M. Palin. 2016. "Activity-Composition Relations for the Calculation of Partial Melting Equilibria in Metabasic Rocks." *Journal of Metamorphic Geology* 34: 845–869.

Guiraud, M., R. Powell, and G. Rebay. 2001. "H_2O in Metamorphism and Unexpected Behaviour in the Preservation of Metamorphc Mineral Assemblages." *Journal of Metamorphic Geology* 19, no. 4: 445–454.

Halpin, J. A., G. L. Clarke, R. W. White, and D. E. Kelsey. 2007. "Contrasting P-T-T Paths for Neoproterozoic Metamorphism in Macrobertson and Kemp Lands, East Antarctica." *Journal of Metamorphic Geology* 25: 683–701.

Harley, S. L. 1989. "The Origins of Granulites: A Metamorphic Perspective." *Geological Magazine* 126, no. 3: 215–247.

Hasterok, D., M. Gard, and J. Webb. 2018. "On the Radiogenic Heat Production of Metamorphic, Igneous, and Sedimentary Rocks." *Geoscience Frontiers* 9, no. 6: 1777–1794. Reliability Analysis of Geotechnical Infrastructures.

Holland, T. 2009. "Ax: A Program to Calculate Activities of Mineral End-Members From Chemical Analyses." accessed November 18, 2021. http://www.esc.cam.ac.uk/research/research-groups/holland/ax.

Holland, T., and J. Blundy. 1994. "Non-Ideal Interactions in Calcic Amphiboles and Their Bearing on Amphibole-Plagioclase Thermometry." *Contributions Mineralogy and Petrology* 116: 433–447.

Holland, T. J. B., E. C. R. Green, and R. Powell. 2022. "A Thermodynamic Model for Feldspars in $KAlSi_3O_8$-$NaAlSi_3O_8$-$CaAl_2Si_2O_8$ for Mineral

Equilibrium Calculations." *Journal of Metamorphic Geology* 40, no. 4: 587–600. https://onlinelibrary.wiley.com/doi/abs/10.1111/jmg.12639.

Holland, T. J. B., and R. Powell. 2011. "An Improved and Extended Internally Consistent Thermodynamic Dataset for Phases of Petrological Interest, Involving a New Equation of State for Solids." *Journal of Metamorphic Geology* 29: 333–383.

Hollis, J., S. Harley, R. White, and G. Clarke. 2006. "Preservation of Evidence for Prograde Metamorphism in Ultrahigh-Temperature, High-Pressure Kyanite-Bearing Granulites, South Harris, Scotland." *Journal of Metamorphic Geology* 24: 263–279.

Imber, J., R. E. Holdsworth, R. A. Strachan, and C. A. Butler. 2002. "The Initiation and Early Tectonic Significance of the Outer Hebrides Fault Zone, Scotland." *Geological Magazine* 139: 609–619.

Kinny, P., and C. Friend. 1997. "U-Pb Isotopic Evidence for the Accretion of Different Crustal Blocks to Form the Lewisian Complex of Northwest Scotland." *Contributions to Mineralogy and Petrology* 129: 326–340.

Kinny, P., C. Friend, and G. Love. 2005. "Proposal for a Terrane-Based Nomenclature for the Lewisian Gneiss Complex of NW Scotland." *Journal of the Geological Society, London* 162: 175–186.

Kriegsman, L. M. 2001. "Partial Melting, Partial Melt Extraction and Partial Back Reaction in Anatectic Migmatites." *Lithos* 56, no. 1: 75–96. https://www.sciencedirect.com/science/article/pii/S0024493700000608.

Lamb, S., and L. Hoke. 1997. "Origin of the High Plateau in the Central Andes, Bolivia, South America." *Tectonics* 16, no. 4: 623–649. https://agupubs.onlinelibrary.wiley.com/doi/abs/10.1029/97TC00495.

Mason, A. J. 2012. "Major Early Thrusting as a Control on the Palaeoproterozoic Evolution of the Lewisian Complex: Evidence From the Outer Hebrides, NW Scotland." *Journal of the Geological Society* 169, no. 2: 201–212.

Mason, A. 2015. "The Palaeoproterozoic Anatomy of the Lewisian Complex, NW Scotland: Evidence for Two 'Laxfordian' Tectonothermal Cycles." *Journal of the Geological Society, London* 173: 153–169.

Mason, A., R. Parrish, and T. Brewer. 2004. "U-Pb Geochronology of Lewisian Orthogneisses in the Outer Hebrides, Scotland: Implications for the Tectonic Setting and Correlation of the South Harris Complex." *Journal of the Geological Society, London* 161: 45–54.

Miocevich, S. R., A. Copley, and O. M. Weller. 2022. "Testing the Importance of Sagduction: Insights From the Lewisian Gneiss Complex of Northwest Scotland." *Precambrian Research* 379: 106708. https://www.sciencedirect.com/science/article/pii/S0301926822001528.

Peach, B. N., J. Horne, W. Gunn, C. T. Clough, L. Hinxman, and H. M. Cadell. 1907. "The Geological Structure of the North West Highlands of Scotland." Memoirs of the Geological Survey of Great Britain.

Powell, R., and T. J. B. Holland. 1988. "An Internally Consistent Dataset With Uncertainties and Correlations: 3. Applications to Geobarometry, Worked Examples and a Computer Program." *Journal of Metamorphic Geology* 6, no. 2: 173–204.

Riel, N., B. J. P. Kaus, E. C. R. Green, and N. Berlie. 2022. "Magemin, an Efficient Gibbs Energy Minimizer: Application to Igneous Systems." *Geochemistry, Geophysics, Geosystems* 23, no. 7: e2022GC010427. https://agupubs.onlinelibrary.wiley.com/doi/abs/10.1029/2022GC010427.

Rosenberg, C. L., and M. R. Handy. 2005. "Experimental Deformation of Partially Melted Granite Revisited: Implications for the Continental Crust." *Journal of Metamorphic Geology* 23, no. 1: 19–28. https://onlinelibrary.wiley.com/doi/abs/10.1111/j.1525-1314.2005.00555.x.

Rubenach, M. J. 1992. "Proterozoic Low-Pressure/High-Temperature Metamorphism and an Anticlockwise P-T Path for the Hazeldene Area, Mount Isa Inlier, Queensland, Australia." *Journal of Metamorphic Geology* 10, no. 3: 333–346. https://onlinelibrary.wiley.com/doi/abs/10.1111/j.1525-1314.1992.tb00088.x.

Sandiford, M., and R. Powell. 1986. "Deep Crustal Metamorphism During Continental Extension: Modern and Ancient Examples." *Earth and Planetary Science Letters* 79: 151–158.

Santosh, M., and K. Sajeev. 2006. "Anticlockwise Evolution of Ultrahigh-Temperature Granulites Within Continental Collision Zone in Southern India." *Lithos* 92: 447–464.

Sutton, J., and J. Watson. 1951. "The Pre-Torridonian Metamorphic History of the Loch Torridon and Scourie Areas in the North-West Highlands, and Its Bearing on the Chronological Classification of the Lewisian." *Quarterly Journal of the Geological Society of London* 106: 241–307.

Tracy, R. J. 1982. "Compositional Zoning and Inclusions in Metamorphic Minerals." *Reviews in Mineralogy* 10: 762–775.

Voll, G., J. Topel, D. R. M. Pattison, and F. Seifert. 1991. *Equilibrium and Kinetics in Contact Metamorphism*. Heidelberg: Springer Berlin.

Weller, O. M., A. Copley, W. G. R. Miller, R. M. Palin, and B. Dyck. 2019. "The Relationship Between Mantle Potential Temperature and Oceanic Lithosphere Buoyancy." *Earth and Planetary Science Letters* 518: 86–99. https://www.sciencedirect.com/science/article/pii/S0012821X19302663.

Weller, O. M., T. J. B. Holland, C. R. Soderman, et al. 2024. "New Thermodynamic Models for Anhydrous Alkaline-Silicate Magmatic Systems." *Journal of Petrology* 65, no. 10: egae098. https://doi.org/10.1093/petrology/egae098.

Wells, P. R. A. 1980. "Thermal Models for the Magmatic Accretion and Subsequent Metamorphism of Continental Crust." *Earth and Planetary Science Letters* 46, no. 2: 253–265. https://www.sciencedirect.com/science/article/pii/0012821X80900114.

White, R., R. Powell, and G. Clarke. 2002. "The Interpretation of Reaction Textures in Fe-Rich Metapelitic Granulites of the Musgrave Block, Central Australia: Constraints From Mineral Equilibria Calculations in the System K_2O-FeO-MgO-Al_2O_3-SiO_2-H_2O-TiO_2-Fe_2O_3." *Journal of Metamorphic Geology* 20: 41–55.

White, R. W., R. Powell, and J. Halpin. 2004. "Spatially-Focussed Melt Formation in Aluminous Metapelites From Broken Hill, Australia." *Journal of Metamorphic Geology* 22, no. 9: 825–845.

White, R. W., R. Powell, and T. J. B. Holland. 2001. "Calculation of Partial Melting Equilibria in the System Na_2O-CaO-K_2O-FeO-MgO-Al_2O_3-SiO_2-H_2O (NCKFMASH)." *Journal of Metamorphic Geology* 19, no. 2: 139–153. https://onlinelibrary.wiley.com/doi/abs/10.1046/j.0263-4929.2000.00303.x.

White, R., R. Powell, T. Holland, T. Johnson, and E. Green. 2014. "New Mineral Activity-Composition Relations for Thermodynamic Calculations in Metapelitic Systems." *Journal of Metamorphic Geology* 32: 261–286.

Whitehouse, M. J., and D. Bridgwater. 2001. "Geochronological Constraints on Paleoproterozoic Crustal Evolution and Regional Correlations of the Northern Outer Hebridean Lewisian Complex, Scotland." *Precambrian Research* 105, no. 2: 227–245. https://www.sciencedirect.com/science/article/pii/S0301926800001133.

Whitney, D., and B. Evans. 2010. "Abbreviations for Names of Rock-Forming Minerals." *American Mineralogist* 95: 185–187.

Will, T. M., and E. Schmadicke. 2003. "Isobaric Cooling and Anti-Clockwise P-T Paths in the Variscan Odenwald Crystalline Complex, Germany." *Journal of Metamorphic Geology* 21: 469–480.

Supporting Information

Additional supporting information can be found online in the Supporting Information section.